ELSEVIER

Contents lists available at ScienceDirect

# Harmful Algae

journal homepage: www.elsevier.com/locate/hal





# Microcystin aids in cold temperature acclimation: Differences between a toxic *Microcystis* wildtype and non-toxic mutant

Gwendolyn F. Stark <sup>a</sup>, Robbie M. Martin <sup>a</sup>, Laura E. Smith <sup>a</sup>, Bofan Wei <sup>b</sup>, Ferdi L. Hellweger <sup>c</sup>, George S. Bullerjahn <sup>d</sup>, R.Michael L. McKay <sup>e</sup>, Gregory L. Boyer <sup>b</sup>, Steven W. Wilhelm <sup>a,\*</sup>

- <sup>a</sup> Department of Microbiology, The University of Tennessee, Knoxville, TN, USA
- <sup>b</sup> Department of Chemistry, State University of New York College of Environmental Science and Forestry, Syracuse, NY, USA
- <sup>c</sup> Water Quality Engineering, Technical University of Berlin, Berlin, Germany
- <sup>d</sup> Department of Biological Sciences, Bowling Green State University, Bowling Green, OH, USA
- e Great Lakes Institute for Environmental Research, The University of Windsor, Windsor, ON, Canada

#### ARTICLE INFO

Edited by: Dr. C. Gobler

Keywords: Cyanobacteria Cyanotoxins Transcriptomics Chemostats Oxidative stress

#### ABSTRACT

For *Microcystis aeruginosa* PCC 7806, temperature decreases from 26 °C to 19 °C double the microcystin quota per cell during growth in continuous culture. Here we tested whether this increase in microcystin provided M. aeruginosa PCC 7806 with a fitness advantage during colder-temperature growth by comparing cell concentration, cellular physiology, reactive oxygen species damage, and the transcriptomics-inferred metabolism to a non-toxigenic mutant strain M. aeruginosa PCC 7806  $\Delta mcyB$ . Photo-physiological data combined with transcriptomic data revealed metabolic changes in the mutant strain during growth at 19 °C, which included increased electron sinks and non-photochemical quenching. Increased gene expression was observed for a glutathione-dependent peroxiredoxin during cold treatment, suggesting compensatory mechanisms to defend against reactive oxygen species are employed in the absence of microcystin in the mutant. Our observations highlight the potential selective advantages of a longer-term defensive strategy in management of oxidative stress (i.e., making microcystin) vs the shorter-term proactive strategy of producing cellular components to actively dissipate or degrade oxidative stress agents.

### 1. Introduction

*Microcystis*-dominated harmful algal blooms (HABs) can occur throughout the summer season. For HABs that occur in temperate North American climates, such as Lake Erie, there are seasonal trends between temperature conditions experienced in early June, when temperatures can average 18 °C, compared to those recorded later in the bloom season (August), when surface water temperatures can reach 26 °C (Dick et al., 2021; Peng et al., 2018). As the season progresses and temperatures warm, harmful algal blooms in Lake Erie have shown a trend of becoming less toxic in conjunction with a shift from toxigenic- to non-toxigenic genotypes (Briand et al., 2009; Dick et al., 2021; Rinta-Kanto et al., 2009). The drivers of this genotypic change remain unknown (Wilhelm et al., 2020).

We previously observed that short-term temperature decreases (within the span of a week) can induce a "cool-temperature phenotype" in *Microcystis aeruginosa*, whereby microcystin production increased

(Martin et al., 2020; Peng et al., 2018). Past research on HAB responses to temperature have largely focused on temperature increases due to concerns for a changing global climate (Paerl and Huisman, 2008). However, when considering cold-to-warm seasonal bloom dynamics, understanding microcystin production across seasonal growth temperatures is relevant. Additionally, lakes subject to cooler stream discharge or which receive inputs from glacial or snow water melt can experience reductions in their thermal structure, even in warmer months (Wetzel, 2001). Changes in microcystin production during growth at cooler temperatures remains an understudied component in understanding *Microcystis* bloom ecology (Martin et al., 2020; Peng et al., 2018).

While regulation of the cold stress response in cyanobacteria is complex, both the physical properties of the thylakoid membranes (fluid or rigid) and the redox state of the plastoquinone pool (PQ pool) are involved in either sensing or responding to cold stress (Maksimov, 2017; Mikami et al., 2002; Ritter et al., 2020; Suzuki et al., 2001). In cyanobacteria, the thylakoid membranes house both the photosynthetic and

E-mail address: wilhelm@utk.edu (S.W. Wilhelm).

<sup>\*</sup> Corresponding author.

respiratory electron pathways, which converge at the PQ pool, making its redox status important for regulating electron transfer and energy dissipation processes in the cell (Liu et al., 2012; Ma et al., 2008; Misumi et al., 2015; Williams and Peter, 1989). Microcystins have been implicated to have a redox-related function. Research has shown differences in redox-related protein abundances between toxigenic and mutant strains of *Microcystis aeruginosa* during iron-limitation (Alexova et al., 2016). Furthermore, thiol-groups, important in maintaining redox balance through glutathione and thioredoxin networks, bind to microcystins in vivo (Mullineaux and Rausch, 2005; Zilliges et al., 2011). The redox state of the of the photosynthetic apparatus in *Microcystis* grown under different light intensities was also negatively correlated with the microcystin content per cell (Deblois and Juneau, 2010). Conclusions drawn from these studies suggest microcystin could play a role in redox-mediated metabolism.

Thiol-groups play a role in redox balance, where the presence of a reactive cysteine residue (thiolate) subjects them to post-translational modifications from reactive oxygen (ROS) and nitrogen species (RNS) (Lu and Holmgren, 2014; Sevilla et al., 2019). This property makes thiol-groups important for redox signaling and enzymatic redox regulatory pathways (Lindahl and Kieselbach, 2009). The original hypothesis offered to explain the binding of microcystin to redox-sensitive thiol groups was that it protected proteins and stabilized them from protease degradation/oxidation (Zilliges et al., 2011). However, the idea of in vivo stabilization was not directly substantiated. While binding of microcystin to thiols could play a stabilizing role, another possibility is that binding of microcystin to proteins may interfere with repair or regulatory functions in the cell (Nishiyama et al., 2005; Schuurmans et al., 2018). Microcystins are known to form a covalent linkage with a key thiol in protein phosphatase 1A in eukaryotes, thereby permanently inactivating these regulatory proteins (MacKintosh et al., 1995). Similarly, microcystin has been shown to bind to phycobilisome subunits (Zilliges et al., 2011). It was hypothesized this binding might serve to stabilize the phycobilisomes from protease degradation. However, in nutrient-limiting conditions, phycobilisome degradation via proteases can be beneficial, therefore microcystin binding might instead interfere in these processes (Alexova et al., 2016; Grossman et al., 1998; Zhang et al., 2008). In these situations, binding of microcystin to proteins might alter metabolic activity that is reliant on protease-mediated degradation or on regulation mediated by the reduction/oxidation of thiol-groups. These interactions alone would mean that microcystin could have a multi-functional regulatory role in the cell, which could help explain why various environmental factors can influence microcystin production (Wilhelm and Boyer, 2011).

In continuous cultures of M. aeruginosa PCC 7806, a decrease in temperature from 26 °C to 19 °C induces a two-fold increase in microcystin quota (Martin et al., 2020). Mechanistically, we hypothesized this response was linked to excitation pressure and the production of oxidative stress as a result of constant light at colder temperatures (Maxwell et al., 1994). In our previous study, peak microcystin quotas coincided with cell recovery and the establishment of a new steady-state cell concentration at 19  $^{\circ}$ C. It was unclear if increased microcystin quota was a key acclimation mechanism, and to what extent other mechanisms were involved. Here we tested the effects of cool temperature on M. aeruginosa PCC 7806 vs. the microcystin-free mutant M. aeruginosa PCC7806 \( \Delta mcyB \) (Dittmann et al., 1997). Through comparisons of transcriptional and physiological responses, we identified alternative mechanisms employed by the mutant to acclimate to 19 °C. Our observations support the idea that in the absence of microcystin as a presumed physiological defense against oxidative stress, cells actively work to dissipate energy and degrade oxidative stress compounds that are generated as byproducts of excess light absorption during cold stress. In Microcystis, the trade-offs between defensive vs. active approaches in mediating oxidative stress establish a potential mechanistic foundation, as well as a new hypothesis, for the regularly observed seasonal transition from toxigenic to non-toxigenic strains during bloom succession.

### 2. Methods

#### 2.1. Continuous cultures

M. aeruginosa PCC 7806 was obtained from the Pasteur Culture Collection and has been maintained for the last decade as both active cultures and cryopreserved stocks. Microcystis aeruginosa PCC7806  $\Delta mcyB$  was generated by Dittmann and colleagues (Dittmann et al., 1997) and kindly provided by Professor E. Dittmann in 2016 (University of Potsdam, Germany). To assess gene mutations or transposon insertion/disruption (Steffen et al., 2014), we re-sequenced and closed the genomes of both strains. Any differentially expressed genes discussed in this paper have been examined (along with adjacent intergenic spacer regions) to ensure phenotypic differences were not due to gene mutations occurring during this experiment (Stark et al., 2023). Going forward we refer to these isolates as "wildtype" and "mutant". Chemostat design and construction followed our previous efforts (Martin et al., 2020). Duplicate 1-L chemostats were established for each strain using modified CT medium (Watanabe and Ichimura, 1977), with nitrogen (N) concentrations at 323 µM supplied as a mix of Ca(NO<sub>3</sub>)<sub>2</sub> and KNO<sub>3</sub> (N molar ratio of 1.37:1) (Martin et al., 2020). Phosphorus (P) was supplied as 16.3  $\mu$ M by K<sub>2</sub>HPO<sub>4</sub>, resulting in N:P molar ratios of ~20. Chemostats were maintained in the same incubator at a measured light intensity of  $\sim$ 50 µmol photon m<sup>-2</sup> s<sup>-1</sup>, with a dilution rate of 0.25 d<sup>-1</sup> controlled by independent peristaltic pumps. Chemostats were acclimated to 26 °C, (referred to as the "warm" treatment), and 50  $\mu$ mol photon m<sup>-2</sup> s<sup>-1</sup> for ~6 weeks, to ensure steady-state was achieved. After chemostat cell concentrations remained stable (coefficient of variation for each individual chemostat were all  $\leq$ 5.55 % over a continual six-day period), incubator temperature was lowered to 19 °C, (referred to as the "cold" treatment) and maintained at 19 °C for 11 days before the temperature was returned to 26  $^{\circ}\text{C}$  . Re-acclimation to 26  $^{\circ}\text{C}$  was monitored for one week. Sample collection (details below) occurred around 12:00 PM daily. Light was kept constant throughout the experiment. Temperature was monitored every 15 min with a Hobo Tidbit TempLogger (Onset Computer Corporation) to account for potential temperature fluctuations. At the end of the experiment, chemostat cultures were assessed for contamination by transferring aliquots to LB medium (Bertani, 1952) followed by incubation at 26 °C in the dark.

# 2.2. Cell abundance and size

Culture (1 ml) was collected from each chemostat through a sampling port using a sterile syringe. The samples were diluted ten-fold in fresh CT medium and assayed with a Guava EasyCyteHT flow cytometer (Millipore). Cell concentrations were determined by gating on red fluorescence, a proxy for chlorophyll *a*, and forward scatter, a proxy for size (Martin et al., 2020).

#### 2.3. Measurement of microcystin

Microcystin concentrations were estimated from 50 mL of culture collected daily. Samples were filtered onto 47-mm glass fiber filters (GF-75, Advantec) via vacuum filtration, immediately flash-frozen in liquid nitrogen, then stored at -80 °C until processing. Quantification of microcystin and congeners was completed by LC-MS as outlined in detail at protocols.io (Boyer, 2020).

# 2.4. Measurements of photosynthetic physiology

To assess changes in photo-physiology, 3 mL of chemostat culture was collected daily. Rapid light curves (RLC) using Pulse-Amplitude Fluorometry (Phyto-PAM II, Heinz Walz GmbH) were generated after 60 s of low-light far-red acclimation. Saturation pulse kinetics were checked to ensure a fluorescence peak was achieved before sample processing. For rapid light curves, saturating pulses (5000 µmol photon

 $m^{-1}~s^{-2})$  were applied every 30 s after actinic light exposure. The RLC consisted of 12 actinic light steps, starting at a PAR (µmol photon  $m^{-1}~s^{-2})$  of 1 and ending at 1275 PAR (µmol photon  $m^{-1}~s^{-2})$ . From these rapid light curves, maximum potential quantum efficiency  $(F_{\rm v}/F_{\rm m})$ , nonphotochemical chlorophyll fluorescence quenching (NPQ), and photosystem II excitation pressure (1-qP) estimates were calculated by the Phyto-PAM II software.

#### 2.5. Oxidative stress assessment

For oxidative stress assessment, the green fluorescent probe, 5-(6)-Chloromethyl-2',7'-dichlorodihydrofluorescein diacetate, acetyl ester, (CM-H<sub>2</sub>DCFDA), was used. A working concentration of approximately  $1.15 \times 10^7$  cells was used for the oxidative stress assays. Cells were first pulled from the chemostats and pelleted by centrifugation at 3700 xg for 15 min at 19 °C. Cell pellets were washed and re-suspended in PBS buffer free of KCl and incubated in the dark with 25 µM of 2',7'-dichlorodihydrofluorescein diacetate (CM-H2DCFDA) suspended in dimethylsulfoxide (DMSO) for 60 min at room temperature (Molecular Probes, Invitrogen). After incubation, cells were washed again and resuspended in PBS buffer. Changes in green fluorescence were measured via flow cytometry using a Guava easyCyteHT flow cytometer (ex $_{\lambda} = 485$  nm.  $em_{\lambda} = 535$  nm). Each sample was run for 120 s, or until a maximum of 5000 cells were counted. Control culture green fluorescence (cells without CM-H2DCFDA) was subtracted from cultures incubated with CM-H<sub>2</sub>DCFDA, for net fluorescent gains. Green fluorescence emission is indicative of the thiol-reactive chloromethyl group of the CM-H<sub>2</sub>DCFDA probe reacting with glutathione and other thiols and it's subsequent oxidation by ROS (Invitrogen).

#### 2.6. RNA extraction

Samples (25 mL) were collected daily on 47 mm diameter,  $0.2 \mu m$ nominal pore-size polycarbonate filters and immediately flash-frozen in liquid nitrogen before storage at -80 °C. We selected ten points across the time course (2 wildtype-strain chemostats and 2 mutant-strain chemostats x 10 time points, n = 40) for RNA sequencing based on cell concentration observations (Supplementary Table 1). To extract RNA, we used the acid-phenol chloroform bead-beating method described in (Martin and Wilhelm, 2020) and Turbo DNA-free kit to eliminate contaminating DNA (Invitrogen). Checks for contaminating DNA were completed by PCR (using 515F and 806R primers targeting the 16 s rRNA gene) and visualization on an agarose gel. Where DNA contamination was present (i.e., PCR products observed in the gel), the sample was processed with another round of DNAse and rechecked until no band was present. Final RNA concentrations were determined using a high-sensitivity Qubit RNA assay per manufacturer's instructions (Invitrogen).

#### 2.7. RNA sequencing and sequence analyses

RNA samples were sent to Discovery Life Sciences (previously Hudson Alpha, Huntsville, AL) where sample library prep and Illumina Novaseq 6000 platform sequencing (50 million reads, 150 bp, paired end) were performed after ribosomal RNA reduction. A TruSeq rRNA reduction was performed on all samples *ex-silico*, according to manufacturer protocol. Sequence data was loaded to CLC genomics Workbench (v. 21.0.4) where it was interleaved, filtered, and trimmed using default program settings. Due to the axenic nature of the chemostats, transcriptome RNA-sequencing reads were mapped (length fraction 0.8, similarity fraction 0.9) to the rRNA genes (PCC7806 has two sets of 5S, 16S and 23S genes) from the *Microcystis aeruginosa* PCC7806SL genome to remove ribosomal reads (Zhao et al., 2018). Reads that did not map to rRNA genes were then stringently mapped (length fraction 0.9, similarity fraction 0.9) to the annotated *Microcystis aeruginosa* PCC 7806SL genome (GenBank accession NZ\_CP020771.1, annotated Jan-28–2020)

(Zhao et al., 2018), and normalized to transcripts per million (TPM). Differential expression analysis within each time point (calculated as expression of wildtype vs. expression of mutant at each time point) was performed using CLC's differential expression algorithm. Genes were considered differentially expressed if FDR-corrected p-values were  $\leq$ 0.05 and fold change was  $\geq$ 2. In our supplemental materials, we considered genes with fold changes > 1.5 and FDR p-values < 0.05 for further investigation into genes of interest that had fold changes > 2 and FDR *p*-values < 0.05 in the main text. For downstream analysis of gene function, coding sequences (CDS) from Microcystis aeruginosa PCC7806SL (NZ\_CP020771.1, annotated Jan-28-2020) were supplemented/merged with annotations from KEGG BlastKOALA. Genes of interest (displayed fold change > 2) that were annotated as "hypothetical genes" were run through NCBI's conserved domain protein search and HMMER for protein homology. Reads mapping to genes that were not annotated and that failed to match with a homologous protein search were omitted from downstream analyses. Tables listing differentially expressed genes by RNA-seq time points (T1-T10) are provided in supplemental tables S3-S12. For this study, we discuss results in terms of transcript abundance: we define that as "relative abundance" within the normalized transcriptomes from each time point.

# 2.8. Data visualization and statistical analyses

All statistical analyses were performed using R studio (4.2.1), PRIMER (v.7), or GraphPad Prism (v. 8.0.2). To check sphericity of the data for a repeated measures ANOVA analysis, Phyto-PAM data was analyzed using the Mauchly test in R. If the data did not fit assumptions (p-value from Mauchly test was <0.05), the Geisser Greenhouse correction was used (Greenhouse and Geisser, 1959). Repeated measures and two-way ANOVA were run in GraphPad Prism (v. 8.0.2). GraphPad Prism was used for time point comparisons of the physiological measurements (cell counts,  $F_{\rm v}/F_{\rm m}$  and NPQ) within or between the strains. PRIMER (v.7) was used for non-metric multidimensional scaling (nMDS). Square-root-transformed TPM expression of all genes in the PCC7806SL genome (4889) was used in calculating the similarity matrix used in the nMDS.

# Data availability

All raw paired-read data used in this study is publicly available at NCBI under the BioProjectID PRJNA1008692.

# 3. Results

# 3.1. Cell concentration in chemostats

At 26 °C, wildtype steady-state cell concentration averaged 3.07  $\times$   $10^6$  mL $^{-1}$  (Fig. 1A). When temperature was lowered to 19 °C, growth rate dropped, causing cell concentration to decrease to an average of  $1.76\times10^6$  mL $^{-1}$ . By T5 (168 h), wildtype cell concentration stabilized around 2.04  $\times$   $10^6$  mL $^{-1}$  for the remainder of the cold treatment (T6 through T8). In the mutant strain, a similar trend in growth rate decline and cell concentration was observed (Fig. 1A). At 26 °C, the mutant steady-state concentration averaged 2.46  $\times$   $10^6$  mL $^{-1}$ . Temperature change to 19 °C resulted in an average concentration decline to 1.27  $\times$   $10^6$  mL $^{-1}$ . By T6 ( $\sim$ 192 h), cell concentrations stabilized around 1.39  $\times$   $10^6$  mL $^{-1}$  for the remainder of the cold treatment. When temperature returned to 26 °C at T9, wildtype cell concentration increased to an average of 2.12  $\times$   $10^6$  mL $^{-1}$  over 24 h, while the mutant cell concentration increased to an average of 1.88  $\times$   $10^6$  mL $^{-1}$  at T9 (336 h).

# 3.2. Cellular microcystin content

Microcystin concentrations in wild-type cells were highly reproducible between the paired chemostats (largest difference  $\pm$  17 %) and

G.F. Stark et al. Harmful Algae 129 (2023) 102531

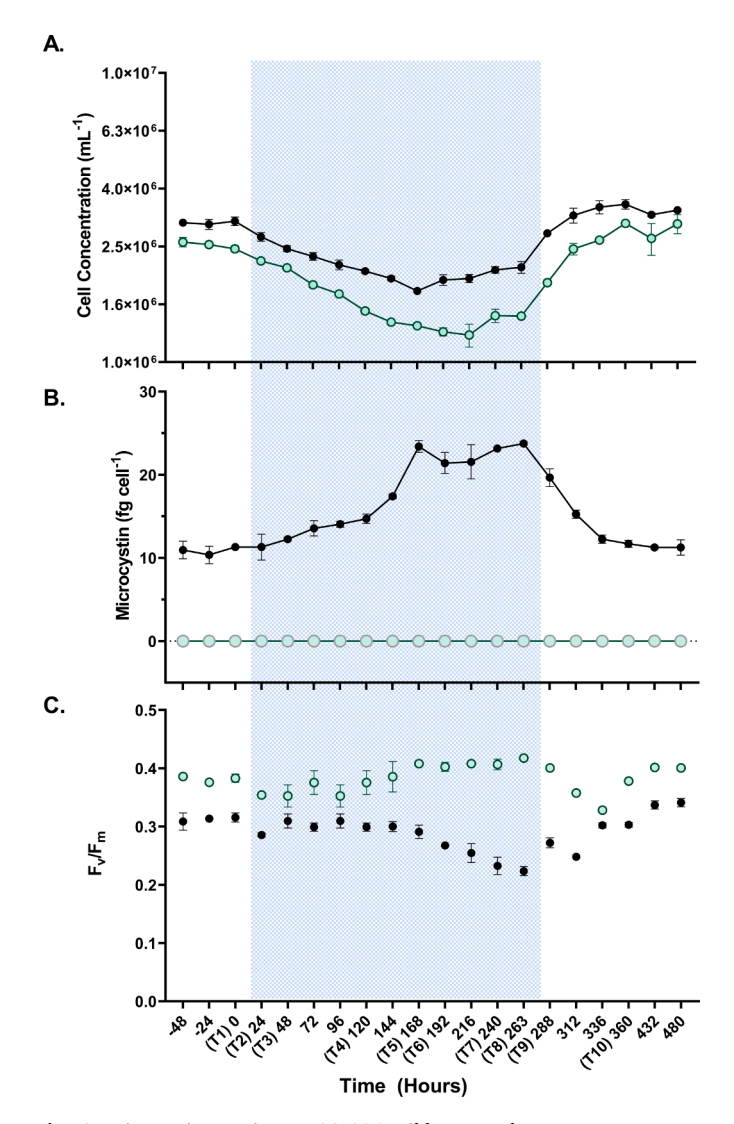


Fig. 1. Microcystis aeruginosa PCC7806 wild-type and mutant responses to temperature change. (A) Average cell concentrations from duplicate wildtype and mutant mono-culture chemostats. Mutant strain is represented by the green open circles, wildtype is represented by black closed circles. Blue shading indicates the 19  $^{\circ}\text{C}$  cold period, white is indicative of the 26  $^{\circ}\text{C}$  warm period. The x-axis is in units of hours, with each of the ten RNA-seq time points. (B) Average microcystin quota in fg/cell from the duplicate wildtype and mutant monoculture chemostats. The mutant strain had no detectable microcystins. The wildtype microcystin quota roughly doubled after 168 h (T5) in cold treatment. The increased microcystin quota persisted in the wildtype for the rest of the cold treatments (T5-T8). (C) Average maximum quantum yield of PSII (F<sub>v</sub>/F<sub>m</sub>) from duplicate wildtype and mutant monoculture chemostats. The mutant shows a steady significant increase in  $F_{\nu}/F_{m}$  during cold treatment by T8 in comparison to T1 (p = 0.046). The wildtype strain  $F_v/F_m$  shows an inverse trend from the mutant, significantly decreasing by T8 compared to T1 (p < 0.0001). In response to the temperature change back to 26 °C, the mutant F<sub>v</sub>/F<sub>m</sub> significantly declined at 312 h (p = 0.044) and 336 h (p = 0.004), compared to  $F_{\nu}/F_{m}$  taken at T9. (For interpretation of the references to color in this figure legend, the reader is referred to the web version of this article.).

reached steady-state concentrations of  $\sim$ 10 fg cell<sup>-1</sup> at 26 °C (Fig. 1B). After temperature decreased to 19 °C, toxin concentration peaked at T5, reaching 23.4 fg cell<sup>-1</sup>. Microcystin remained elevated (>20 fg cell<sup>-1</sup>) in the wildtype for the duration of the cold period (T6-T8). When the temperature returned to 26 °C, toxin declined to pre-cold-treatment levels. No microcystins were detected in  $\Delta$ mcyB cultures (Fig. 1B). Though no toxin was produced in the mutant, transcription of mcyD and mcyA followed the expression pattern of the wildtype strain throughout

our RNA-seq time series (Fig. S1A-B).

# 3.3. Photosynthetic physiology assessment

In the wildtype,  $F_v/F_m$  values stayed consistent throughout the cold treatment, until T6 (~192 h) (Fig. 1C). At T6,  $F_v/F_m$  values decreased, becoming significantly lower at T7 (~240 h) (p=0.038) and T8 (~263 h) (p<0.0001) compared to T1 (0 h). In the mutant,  $F_v/F_m$  was consistently higher than the wildtype, regardless of treatment (Fig. 1C). During the cold treatment,  $F_v/F_m$  in the mutant was higher at T6 (p=0.016) and T8 (p=0.046) than at T1 (Fig. 1C).

The mutant and wildtype responded differently during reacclimation to 26 °C.  $F_v/F_m$  declined significantly in the mutant in the 48 h period after the temperature was returned to 26 °C (T9 vs. 312 h, p=0.044; T9 vs. 336 h, p=0.004) (Fig. 1C). In contrast, in the wildtype,  $F_v/F_m$  increased in the same 48 h period, but the increase was not significant compared to T9.

Non-photochemical quenching (NPQ) measurements were derived from the rapid light curves (Fig. 2). In the wildtype, there were no significant differences in NPQ measurements during the cold treatment (T5) compared the control (T1) (Fig. 2). In the mutant, there was a significant increase in NPQ measurements taken during the cold treatment (T5) compared to the control (T1). These increases occurred at all PAR (µmol photon m $^{-2}$  s $^{-1}$ ) values >345 (Holm-Sidak p $_{\rm adj}$  all <0.05) (Fig. 2, Fig. S2). At T1, the mutant had higher NPQ than the WT across all PAR intensities measured, but the differences were not significant. However, NPQ was significantly higher in the mutant at T5 at all seven measured PAR values ( $p=0.024,\,0.005,\,0.001,\,0.006,\,0.008,\,0.005,\,0.003$ ). These data suggest differences in acclimation strategies between the two strains.

To assess stress on photosystem II at T5 versus control timepoints (T1 and T10), excitation pressure measurements were derived from the rapid light curves (Fig. S3). The wildtype had significantly higher excitation pressure at T5, compared to T1 and T10 (p = 0.0161, 0.0120). The mutant had significantly higher excitation pressure at T5 versus T10 (p = 0.0087).

# 3.4. Reactive oxygen species measurements via the CM-H<sub>2</sub>DCFDA assay

The CM-H<sub>2</sub>DCFDA assay revealed significantly higher net green fluorescence (p < 0.0001) in the mutant compared to the wildtype strain during the eleven-day cold temperature treatment period (Fig. S4A-B). There was no significant difference in net green fluorescence between the strains during growth at 26 °C.

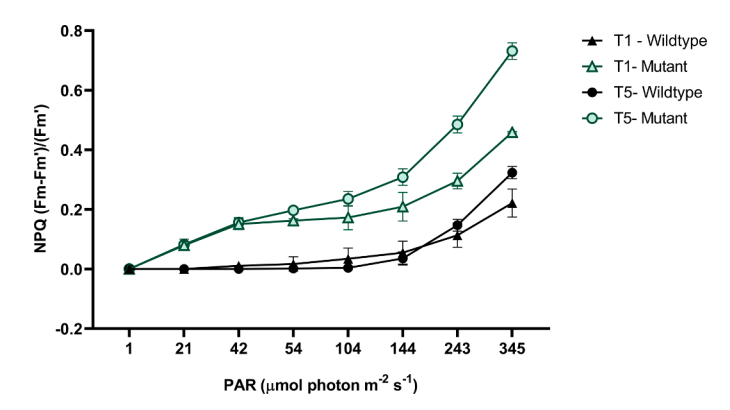


**Fig. 2.** Average non-photochemical quenching measurements (NPQ) collected from the rapid light curves (RLC) for each chemostat, at T1 (0 h) and T5 ( $\sim$ 168 h). NPQ significantly differs between the mutant and wildtype for measurements taken at the T5 time point across all actinic PAR (µmol photons m $^{-2}$  s $^{-1}$ ) measured (Holm sidak adj. p-values = 0.024, 0.005, 0.001, 0.006, 0.008, 0.005, 0.003). (For interpretation of the references to color in this figure legend, the reader is referred to the web version of this article.).

# 3.5. Transcriptional profiles for control, cold treatment, and cold-recovery

The transcriptional profiles of chemostat populations from ten time points is provided in Table S1. We sequenced 40 mRNA libraries with total reads ranging from 25,573,750 to 78,079,140 per library (Table S2). Broad transcriptional patterns were determined by projecting samples in two-dimensional space (nMDS) based on the expression of all genes in each genome (Fig. 3). This nMDS representation resulted in a circular progression across measured time points (T1-T10). In both strains, T2-T9 scale away from T1 in a counter-clockwise pattern, showing an increasing divergence in gene expression during cold acclimation. However, the mutant transcriptomes diverge from T1 more than the wildtype. *Re*-acclimation to 26 °C (T10) resulted in the transcriptional profile returning to a state similar to T1 in both strains.

Transcriptomic differences between the mutant and wildtype in warm conditions (T1 and T10). There were 61 differentially expressed genes (fold change  $\geq 2$ ) at T1 and 94 at T10, many of which (42 genes) overlapped. A significant finding was differential expression of genes located in a putative gene cluster (gene cluster 1) with homology to transmembrane proteins, and genes with functions related to redox metabolism/membrane potential (Table S13). At T1, all genes from gene cluster 1 were upregulated 4.6–22.8-fold (all p < 0.001) in the mutant strain (Fig. S5, Table S3). At T10, transcripts from seven of the genes in putative gene cluster 1 were upregulated 2.3–9.1-fold in the mutant (p < 0.001) (Table S12). All other differentially expressed genes at these time points (T1 and T10), and the rest of the RNA seq time points (T2-T9) can be found in Tables S3-S12.

# 3.6. Transcript differences between the mutant and wildtype in cold conditions (T2-T8)

Generally, differences in gene expression during cold growth involved changes in a glutathione-dependent peroxiredoxin, and cytochrome-based electron transport pathways (Figs. 4, 5A-D). Cold treatment produced differential expression of a glutathione-dependent peroxiredoxin (pgdx), which increased in the mutant relative to the wildtype starting at T4. By T5, pgdx showed a 2.1-fold-change increase in the mutant (p < 0.001) (Fig. 4). There was no differential expression (fold change  $\geq$  2) observed for other antioxidant genes (sod, prx) between the strains, however there was a thioredoxin-dependent 2-cys peroxiredoxin (locus tag BH695\_RS02415), which showed fold change

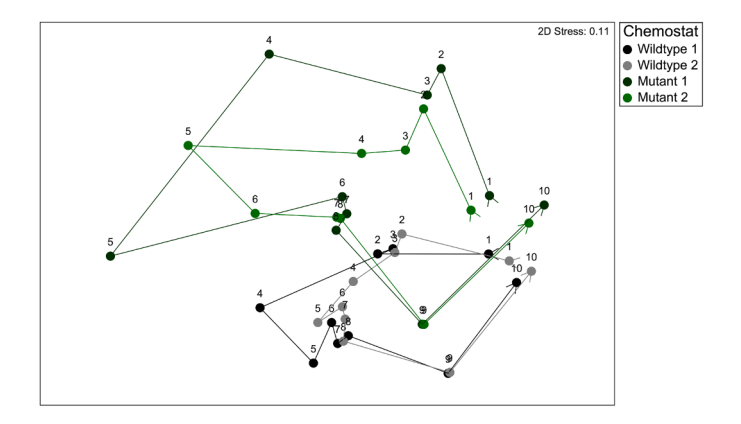


**Fig. 3.** NMDS of square root transformed transcriptomic data, normalized by transcripts per million (TPM), encompassing the whole transcriptome for wildtype (black and gray circles) and mutant (green and dark green circles) monoculture chemostats, n=40. The nMDS was constructed to see how the transcriptomes changed over time throughout the cold temperature treatment at each RNA- seq timepoint (T1 through T10). (For interpretation of the references to color in this figure legend, the reader is referred to the web version of this article.).

#### pgdx (glutathione-dependent peroxiredoxin)

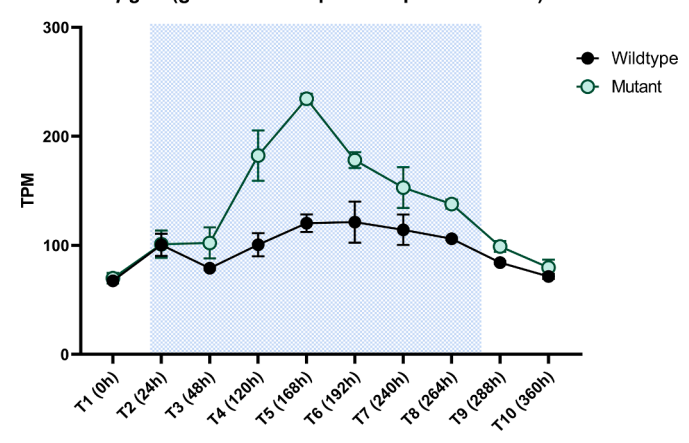


**Fig. 4.** Average transcriptomic data normalized by transcript per million (TPM), for the mutant (green circles) and wildtype (black circles) for the glutathione-dependent peroxiredoxin, pgdx. At T5 the mutant shows a 2.14 fold change increase (p < 0.0001) in transcript abundance of pgdx. (For interpretation of the references to color in this figure legend, the reader is referred to the web version of this article.).

increases of  $\geq\!\!1.5$  but < 2 (FDR p<0.0001) from T6-T8 in the mutant (Fig. S6).

In the mutant, a subunit of the photoprotective cytochrome  $b_{559}$  complex in PSII (psbE) and the respiratory pathway based on cytochrome c oxidase (coxBAC) showed differential expression during cold treatment (Fig. 5A-D). From T4 to T8, cytochrome c oxidase expression (coxBAC) increased in the mutant (Fig. 5A-C, Tables S6–10), while cytochrome  $b_{559}$  alpha subunit (psbE), an electron sink, increased  $\sim$ 2-fold, (p < 0.001) at T5 (Fig. 5D). Based on psbE and coxBAC expression, the mutant had increased expression of thylakoid-membrane-associated electron sinks during cold acclimation.

We also saw changes in expression for genes pntA (2 copies), pntB, petJ, and petE, all of which are associated with proton/electron transporting processes. The genes pntA (both copies), pntB and petJ did not meet our criteria of fold changes  $\geq 2$ , instead they showed fold changes  $\geq 1.5$  but < 2, with FDR-adjusted p-values < 0.0001 from T6-T8 (Fig. S7, and S8A). The electron transporter, plastocyanin (petE), showed fold change decreases > 2 (FDR-adjusted p < 0.0001) from T7-T9 in the mutant (Fig. S8B).

# 4. Discussion

The purpose of this study was to determine if changes in microcystin production provided an advantage to Microcystis aeruginosa PCC 7806 in its response to cold stress. Here we used cold acclimation under constant light - conditions known to generate oxidative stress in phototrophs (Gray et al., 1996; Huner et al., 1998; Maxwell et al., 1994). We compared the response of non-toxigenic PCC 7806 \( \Delta mcyB \) (Dittmann et al., 1997) with its corresponding toxic wild-type. These strains were chosen to allow comparison within the most genetically similar backgrounds (e.g., Van de Waal et al., 2011). We note that over time, genetic changes have accumulated between the two strains (Stark et al., 2023). As part of this study, we validated that genes individually reported herein as differentially expressed were consistent in terms of genomic structure between strains. Genes that were identified as mutated were not considered in our gene expression analysis within the main text or supplemental figures. The physiology of the wildtype and mutant strains were monitored with various methods during growth in chemostats shifted from 26 °C to 19 °C to induce cold stress (vis a vis Martin et al., 2020), a condition known to induce microcystin production. By pairing the temporal RNA-seq analyses with photo-physiology and ROS measurements, we have identified differences in how a toxigenic vs.

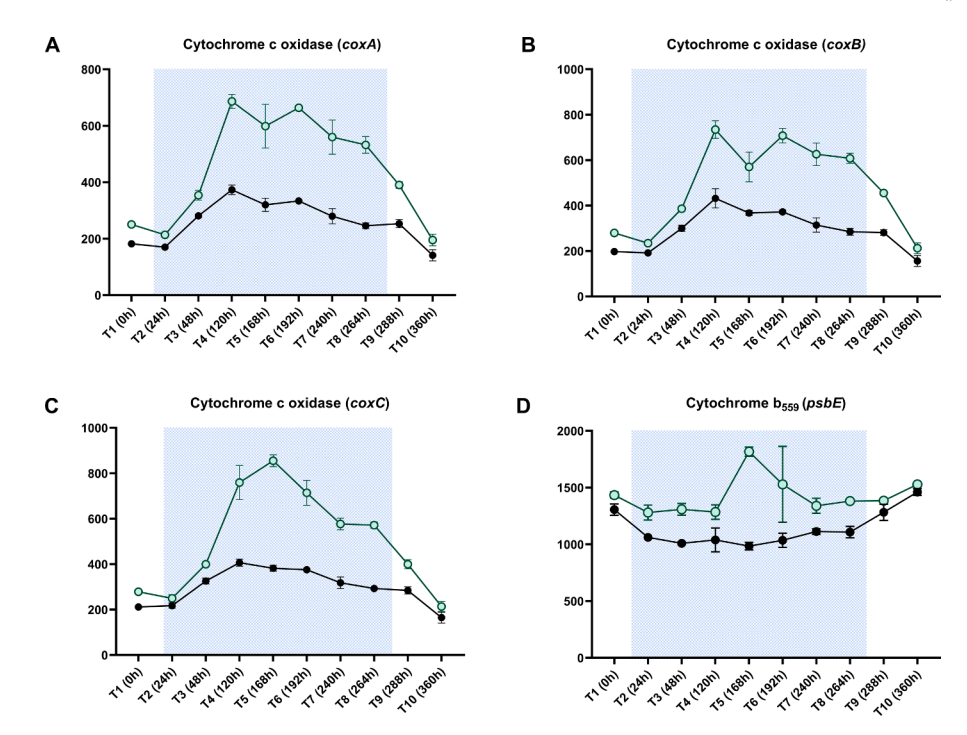


**Fig. 5.** Transcriptomic data, normalized by transcript per million (TPM), for the mutant (green circles) and wildtype (black circles) for cytochrome c oxidase, coxBAC. The x-axis shows each RNA-seq time point in order, from time 0 to 360 h. (A) Starting at T4, coxA shows a fold change increase of 2.1 (p < 0.0001). This fold change increase >2 of coxA is seen through the rest of the cold treatment period (T5-T8) (Supplementary tables dataset). (B) Starting at T4, coxC shows a fold change increase of 2.1(p < 0.001) in the mutant. This fold change increase >2 of coxC is seen through the rest of the cold treatment period (T5-T8) (Supplementary tables dataset). (C) At T6, coxB shows fold change increase of 2.15 (p < 0.0001) in the mutant, fold change >2 of this gene is maintained through T7 and T8 in the mutant (Tables S9-S10). (D) In the mutant, cytochrome  $b_{559}$  (psbE) saw a fold change increase of 2.04, with p < 0.0001 at T5. (For interpretation of the references to color in this figure legend, the reader is referred to the web version of this article.).

non-toxigenic strain responds and recovers to cool temperature exposure. We present these observations couched within a framework that describes how microcystin influences cell physiology and distinguishes between a defensive role microcystin may play in redox-homeostasis vs. the mutant's active metabolic restructuring to increase electron sink capacity and degrade ROS.

Microcystin has been implicated as playing a role in the oxidative stress response, due to its thiol-binding abilities (Schuurmans et al., 2018; Zilliges et al., 2011). Oxidative stress can be generated by photosynthetic processes in cyanobacteria, where disruptions in the redox state of the thylakoid membranes can increase ROS generation if electron source exceeds electron sink capacity. During the cold temperature treatment, we observed a general trend of more ROS in the mutant via our CM-H<sub>2</sub>DCFDA assay compared to the wildtype (Fig. S4). Interestingly, we also observed an increase in expression of a glutathione-dependent peroxiredoxin (pgdx) in the mutant a week (T5) into cold treatment, which coincides with microcystin quota peaking and cell concentration recovery in the wildtype (mutant cold recovery was slightly delayed and started at T6). Glutathione-dependent peroxiredoxins are important for H<sub>2</sub>O<sub>2</sub> detoxification and have also been implicated as acting as redox sensors (Chae et al., 2012; Dietz et al., 2008). Differential expression of pdgx in the mutant during cold treatment is indicative of intracellular stress conditions absent in the wildtype. While other ROS scavengers, such as superoxide dismutase and other peroxiredoxins, behaved similarly in the mutant and wildtype (no fold change > 2), the behavior of pgdx might indicate more specific regulatory activity than just ROS detoxification alone. Thus, while ROS protection may be one role of microcystin in the cell, the specifics as to the type or location of ROS-inducing damage (H<sub>2</sub>O<sub>2</sub> v. O<sup>-</sup>) needs more attention.

Glutathione-dependent peroxiredoxins are reliant on glutathione reductase activity, whose disulfide reductase activity is powered by NADPH (Deponte, 2013; Lu and Holmgren, 2014). Microcystin is

capable of binding to glutathione reductase in vivo, and it has been hypothesized this binding might either aid or interfere in the oxidative stress response (Schuurmans et al., 2018; Zilliges et al., 2011). While it is possible the presence of microcystin could be altering the activity of pgdx in the wildtype, broader implications of microcystin interference with the glutathione/thioredoxin networks might mean that less NADPH is required for cold metabolism in the wildtype, a scenario consistent with the decreased  $F_v/F_m$  beginning at T7. This reduction in  $F_v/F_m$  came with no impediment to wildtype growth. Conversely, the mutant not only showed increased  $F_v/F_m$  later into the cold treatment, but there was also an increase in transcription of an NADPH transhydrogenase (pntAB) in the mutant relative to the wildtype from T5 through T8 (Fig. S7). This may indicate the mutant takes more action to properly maintain NAD (P)+/NAD(P)H pools during cold growth, which could signify differences in redox coupling of these cofactors and intracellular redox homeostasis in the mutant (Kämäräinen et al., 2017).

We saw additional transcriptional and photo-physiological evidence of metabolic "re-wiring" in the mutant to acclimate to the cold, around the same time pgdx gene expression peaked. The mutant upregulated cytochrome b<sub>559</sub> (psbE) and cytochrome c oxidase (coxBAC) in what we interpret as an effort to increase electron sink capacity. Cytochrome b<sub>559</sub> has been shown to aid in photoprotection, by acting as an alternate electron pathway (Hamilton et al., 2014). Cytochrome c oxidase (cox-BAC) is a respiratory terminal oxidase that generates ATP by consuming oxygen and NAD(P)H reducing equivalents (Lea-Smith et al., 2016). However, cytochrome c oxidase serves a dual role in the cell, both increasing ATP generation and having a photoprotective role, where it acts as an additional electron sink by diverting electrons away from the donor side of photosystem I via plastocyanin or cytochrome c<sub>6</sub> (Lea--Smith et al., 2016; Nikkanen et al., 2021). Because of this, it is thought that activity of this complex in the light may be regulated by the redox state of the electron carriers plastocyanin and cytochrome c<sub>6</sub> (Ermakova et al., 2016). Differential expression of these two electron transporters G.F. Stark et al. Harmful Algae 129 (2023) 102531

was observed in the mutant during the cold treatment (Fig. S8A-B). In terms of photoprotective abilities, there was an inverse trend of the pgdx expression with cytochrome c oxidase and cytochrome  $b_{559}$  expression. This gives more credibility to the hypothesis that they are upregulated to help modulate thylakoid redox state in the mutant, until cold acclimation and cell recovery occur around T6, after which their expression begins to decline. Additionally, cytochrome c oxidase relies on NAD(P)H for proton translocation, which further supports an increased need (or may function as a sink) for NAD(P)H in the mutant during cold temperature growth.

Based on transcriptional data presented, we conclude that the mutant and wildtype allocate excitation energy differently. Our NPQ data support this. The mutant had higher NPQ at all incident PAR at T5 compared to the wildtype. This means that during cold growth, the mutant would be more reliant on photo-protective energy dissipation through non-photochemical quenching, which can be achieved either by the orange carotenoid protein in photosystem II or state transitions (Boulay et al., 2008; Campbell and Oquist, 1996). Increasing electron sinks and induction of NPQ processes in the mutant would decrease generation of ROS, which can result from an over-reduced thylakoid membrane (Gao and Erdner, 2022; Kanervo et al., 2005). This is interesting, as the excitation pressure of PSII significantly increases in the wildtype at T5 (compared to controls T1 and T10) (Fig. S3). However, the wildtype manages this without increasing alternate electron pathways, or in the short term without increasing NPQ, and still recovers during cold growth despite reduced F<sub>v</sub>/F<sub>m</sub> after this time. When taken together, these findings show that the mutant and wildtype have different energy dissipation capabilities during cold growth, which may affect NAD(P)+/NAD(P)H pools or the thylakoid membranes. The absence of microcystin in the mutant increases the need for electron dissipating pathways, indicating microcystin may play a role in processes related to the photosynthetic electron transport chain. Complementary to this idea, if the mutant employs these strategies to mitigate or reduce ROS production, the absence of "turning on" these strategies in the wildtype could mean microcystin is in fact playing a role in the oxidative stress response, as has been previously hypothesized by other researchers.

# 4.1. Microcystin production alters cold stress management strategies

In response to cold treatment (11 days), the non-toxigenic mutant upregulated a glutathione-dependent peroxiredoxin and a cytochrome c oxidase complex, both of which help mitigate or reduce ROS generation in cyanobacteria. These responses temporally coincided with an increase of microcystin in the wildtype. Coincident in time, photo-acclimation strategies differed, in which the strains showed opposite response in F<sub>v</sub>/F<sub>m</sub>, and NPQ measurements increased in the mutant. This implies cold acclimation alters electron transport capabilities differently in the mutant and wildtype strains. Our NPQ measurements also indicate inherent differences in the redox state of the thylakoid membranes between the strains during cool temperatures (Misumi et al., 2015). Indeed, differences in redox-related proteins have been shown to differ between these strains, and conditions that can cause over reduction of the thylakoid membranes, such as high-light growth, provide the toxigenic strain an advantage (Alexova et al., 2016, 2011; Phelan and Downing, 2011). Collectively, our observations lead to the idea that increased microcystin per-cell during the cold treatment may provide a longer-term benefit (days versus hours) during conditions which can stress photosynthetic metabolism resulting in more ROS generation (here brought on by cold temperature growth). This leads us to our hypothesis that in locations that experience seasonal temperature trends like Lake Erie, microcystin quota may be higher under conditions where solar days are longer, and the water is clearer and colder (e.g., June). This phenomenon may be overlooked by total microcystin measurements (µg/L) alone, as overall biomass is lower earlier in the growing season, and may be better observed with per-cell toxin quotas. The

replacement of microcystin producers by non-producers in August (where temperatures are warmer, solar days shorter and water less clear) occurs during periods that may favor photo acclimation strategies that differ from those seen during high light and low temperature growth periods. This would include the use of enzymes that directly degrade reactive oxygen (e.g., like peroxiredoxin), noting that specific strategies may be tailored to certain reactive oxygen species. Thus, there could be a connection between photo acclimation strategies for Microcystis, the nature of the photosynthetic stressors, and succession of toxigenic genotypes of Microcystis. We hypothesize that trade-offs in the differing strategies of managing photosynthetic stressors may therefore play an important role in regulating/selecting the toxigenic composition of Microcystis blooms (although other factors are also likely playing a role) (Chaffin et al., 2023). Agent-based modeling has suggested that nitrogen availability may contribute to the succession of toxigenic to non-toxigenic strains in Lake Erie (Hellweger et al., 2022). Data from our experiment can be integrated into such models, allowing us to quantify how nutrients and temperature contribute to genotypic succession. Doing so may help improve management and mitigation strategies of *Microcystis*-dominated harmful algal blooms. Yet it is important to acknowledge that Microcystis blooms are complicated: the influence (s) of other environmental factors as well as competition with biology needs to be appropriately accounted for in our stewardship of lake systems.

# CRediT authorship contribution statement

Gwendolyn F. Stark: Conceptualization, Data curation, Formal analysis, Investigation, Methodology, Validation, Visualization, Writing – original draft, Writing – review & editing. Robbie M. Martin: Conceptualization, Methodology, Writing – review & editing. Laura E. Smith: Investigation, Writing – review & editing. Bofan Wei: Investigation, Writing – review & editing. Ferdi L. Hellweger: Funding acquisition, Writing – review & editing. George S. Bullerjahn: Funding acquisition, Writing – review & editing. R.Michael L. McKay: Writing – review & editing. Gregory L. Boyer: Resources, Supervision, Writing – review & editing. Steven W. Wilhelm: Conceptualization, Formal analysis, Funding acquisition, Methodology, Project administration, Resources, Supervision, Writing – review & editing.

# **Declaration of Competing Interest**

The authors declare that they have no known competing financial interests or personal relationships that could have appeared to influence the work reported in this paper.

# Data availability

All data has been made available either in the article or uploaded to public repositories.

# Acknowledgements

This work was supported by funds from the National Science Foundation (OCE-1840715) and the National Institute of Environmental Health Sciences (1P01ES028939–01) through funds provided to the Great Lakes Center for Fresh Waters and Human Health at Bowling Green State University, and the National Oceanographic and Atmospheric Administration (NA18NOS4780175, ECOHAB contribution #1086). We also thank the generous support of the Kenneth & Blaire Mossman Endowment to the University of Tennessee.

# Supplementary materials

Supplementary material associated with this article can be found, in

the online version, at doi:10.1016/j.hal.2023.102531.

#### References

- Alexova, R., Dang, T.C., Fujii, M., Raftery, M.J., Waite, T.D., Ferrari, B.C., Neilan, B.A., 2016. Specific global responses to N and Fe nutrition in toxic and non-toxic *Microcystis aeruginosa*. Environ. Microbiol. 18 (2), 401–413.
- Alexova, R., Haynes, P.A., Ferrari, B.C., Neilan, B.A., 2011. Comparative protein expression indifferent strains of the bloom-forming cyanobacterium *Microcystis aeruginosa*. Mol. Cell. Proteomics 10 (9). M110.003749.
- Bertani, G., 1952. Studies on Lysogenesis. I. The mode of phage liberation by lysogenic Escherichia coli. J. Bacteriol. 62, 293–300.
- Boulay, C., Abasova, L., Six, C., Vass, I., Kirilovsky, D., 2008. Occurrence and function of the orange carotenoid protein in photoprotective mechanisms in various cyanobacteria. Biochimica et Biophysica Acta (BBA) - Bioenergetics 1777 (10), 1344–1354.
- Boyer, G.L., 2020. LCMS-SOP Determination of microcystins in water samples by high performance liquid chromatography (HPLC) with single quadrupole mass spectrometry (MS), protocols.io. doi: 10.17504/protocols.io.bck2iuye.
- Briand, E., Escoffier, N., Straub, C., Sabart, M., Quiblier, C., Humbert, J.-F., 2009. Spatiotemporal changes in the genetic diversity of a bloom-forming *Microcystis aeruginosa* (cyanobacteria) population. ISME J. 3 (4), 419–429.
- Campbell, D., Oquist, G., 1996. Predicting light acclimation in cyanobacteria from nonphotochemical quenching of photosystem II fluorescence, which reflects state transitions in these organisms. Plant Physiol. 111 (4), 1293–1298.
- Chae, H.Z., Oubrahim, H., Park, J.W., Rhee, S.G., Chock, P.B., 2012. Protein glutathionylation in the regulation of peroxiredoxins: a family of thiol-specific peroxidases that function as antioxidants, molecular chaperones, and signal modulators. Antioxid. Redox Signal. 16 (6), 506–523.
- Chaffin, J.D., Westrick, J.A., Reitz, L.A., Bridgeman, T.B., 2023. Microcystin congeners in Lake Erie follow the seasonal pattern of nitrogen availability. Harmful Algae 127, 102466.
- Deblois, C.P., Juneau, P., 2010. Relationship between photosynthetic processes and microcystin in *Microcystis aeruginosa* grown under different photon irradiances. Harmful Algae 9, 18–24.
- Deponte, M., 2013. Glutathione catalysis and the reaction mechanisms of glutathione-dependent enzymes. Biochim. Biophys. Acta 1830 (5), 3217–3266.
- Dick, G.J., Duhaime, M.B., Evans, J.T., Errera, R.M., Godwin, C.M., Kharbush, J.J., Nitschky, H.S., Powers, M.A., Vanderploeg, H.A., Schmidt, K.C., Smith, D.J., Yancey, C.E., Zwiers, C.C., Denef, V.J., 2021. The genetic and ecophysiological diversity of *Microcystis*. Environ. Microbiol. 23 (12), 7278–7313.
- Dietz, K.-J., Stork, T., Finkemeier, I., Lamkemeyer, P., Li, W.-X., El-Tayeb, M.A., Michel, K.-P., Pistorius, E., Baier, M., 2008. The role of peroxiredoxins in oxygenic photosynthesis of cyanobacteria and higher plants: peroxide detoxification or redox sensing? In: Garab, G. (Ed.), Advances in Photosynthesis and Respiration. Springer, Netherlands, pp. 303–319.
- Dittmann, E., Neilan, B.A., Erhard, M., von Dohren, H., Borner, T., 1997. Insertional mutagenesis of a peptide synthetase gene that is responsible for hepatotoxin production in the cyanobacterium *Microcystis aeruginosa* PCC 7806. Mol. Microbiol. 26, 779–787.
- Ermakova, M., Huokko, T., Richaud, P., Bersanini, L., Howe, C.J., Lea-Smith, D., Peltier, G., Allahverdiyeva, Y., 2016. Distinguishing the roles of thylakoid respiratory terminal oxidases in the cyanobacterium *Synechocystis sp.* PCC 6803. Plant Physiol. 171, 1307–1319.
- Gao, Y., Erdner, D.L., 2022. Cell death responses to acute high light mediated by non-photochemical quenching in the dinoflagellate *Karenia brevis*. Sci. Rep. 12 (1), 14081.
- Gray, G.R., Savitch, L.V., Ivanov, A.G., Huner, N., 1996. Photosystem II excitation pressure and development of resistance to photoinhibition (II. Adjustment of photosynthetic capacity in Winter Wheat and Winter Rye). Plant Physiol. 110 (1), 61–71.
- Greenhouse, S.W., Geisser, S., 1959. On methods in the analysis of profile data. Psychometrika 24 (2), 95–112.
- Grossman, A.R., Schwarz, R., Bhaya, D., Dolganov, N., 1998. Phycobilisome degradation and responses of cyanobacteria to nutrient limitation and high light. In: Garab, G. (Ed.), Photosynthesis: Mechanisms and Effects. Springer, Netherlands, pp. 2853–2858.
- Hamilton, M.L., Franco, E., Deak, Z., Schlodder, E., Vass, I., Nixon, P.J., 2014. Investigating the photoprotective role of cytochrome b-559 in photosystem II in a mutant with altered ligation of the haem. Plant Cell Physiol. 55 (7), 1276–1285.
- Hellweger, F.L., Martin, R.M., Eigemann, F., Smith, D.J., Dick, G.J., Wilhelm, S.W., 2022. Models predict planned phosphorus load reduction will make Lake Erie more toxic. Science 376, 1001–1005.
- Huner, N.P.A., Öquist, G., Sarhan, F., 1998. Energy balance and acclimation to light and cold. Trends Plant Sci. 3 (6), 224–230.
- Kämäräinen, J., Huokko, T., Kreula, S., Jones, P.R., Aro, E.M., Kallio, P., 2017. Pyridine nucleotide transhydrogenase PntAB is essential for optimal growth and photosynthetic integrity under low-light mixotrophic conditions in *Synechocystis* sp. PCC6803. New Phytol. 214 (1), 194–204.
- Kanervo, E., Suorsa, M., Aro, E.-M., 2005. Functional flexibility and acclimation of the thylakoid membrane. Photochem. Photobiol. Sci. 4 (12), 1072–1080.
- Lea-Smith, D.J., Bombelli, P., Vasudevan, R., Howe, C.J., 2016. Photosynthetic, respiratory and extracellular electron transport pathways in cyanobacteria. Biochim. Biophys. Acta 1857 (3), 247–255.

- Lindahl, M., Kieselbach, T., 2009. Disulphide proteomes and interactions with thioredoxin on the track towards understanding redox regulation in chloroplasts and cyanobacteria. J. Proteomics 72 (3), 416–438.
- Liu, L.-N., Bryan, S.J., Huang, F., Yu, J., Nixon, P.J., Rich, P.R., Mullineaux, C.W., 2012. Control of electron transport routes through redox-regulated redistribution of respiratory complexes. Proc. Natl Acad. Sci. 109 (28), 11431–11436.
- Lu, J., Holmgren, A., 2014. The thioredoxin antioxidant system. Free Radic. Biol. Med. 66, 75–87.
- Ma, W., Deng, Y., Mi, H., 2008. Redox of plastoquinone pool regulates the expression and activity of NADPH dehydrogenase supercomplex in *Synechocystis* sp. PCC6803. Curr. Microbiol. 56 (2), 189–193.
- MacKintosh, R.W., Dalby, K.N., Campbell, D.G., Cohen, P.T.W., Cohen, P., MacKintosh, C., 1995. The cyanobacterial toxin microcystin binds covalently to cysteine-273 on protein phosphatase 1. FEBS Lett. 371 (3), 236–240.
- Maksimov, E.G., 2017. Membrane fluidity controls redox-regulated cold stress responses in cyanobacteria. Photosyn. Res. 133, 215–223.
- Martin, R.M., Moniruzzaman, M., Stark, G.F., Gann, E.R., Derminio, D.S., Wei, B., Hellweger, F.L., Pinto, A., Boyer, G.L., Wilhelm, S.W., 2020. Episodic decrease in temperature increases mcy gene transcription and cellular microcystin in continuous cultures of Microcystis aeruginosa PCC 7806. Front. Microbiol. 11, 601864.
- Martin, R.M., Wilhelm, S.W., 2020. Phenol based RNA extraction from polycarbonate filters. protocols.io doi: 10.17504/protocols.io.bivuke6w.
- Maxwell, D.P., Falk, S., Trick, C.G., Huner, N., 1994. Growth at low temperature mimics high-light acclimation in *Chlorella vulgaris*. Plant Physiol. 105 (2), 535–543.
- Mikami, K., Kanesaki, Y., Suzuki, I., Murata, N., 2002. The histidine kinase Hik33 perceives osmotic stress and cold stress in *Synechocystis* sp. PCC 6803. Mol. Microbiol. 46 (4), 905–915.
- Misumi, M., Katoh, H., Tomo, T., Sonoike, K., 2015. Relationship between photochemical quenching and non-photochemical quenching in six species of cyanobacteria reveals species difference in redox state and species commonality in energy dissipation. Plant Cell Physiol. 57 (7), 1510–1517.
- Mullineaux, P.M., Rausch, T., 2005. Glutathione, photosynthesis and the redox regulation of stress-responsive gene expression. Photosyn. Res. 86 (3), 459–474.
- Nikkanen, L., Solymosi, D., Jokel, M., Allahverdiyeva, Y., 2021. Regulatory electron transport pathways of photosynthesis in cyanobacteria and microalgae: recent advances and biotechnological prospects. Physiol. Plant. 173 (2), 514–525.
- Nishiyama, Y., Allakhverdiev, S.I., Murata, N., 2005. Inhibition of the repair of Photosystem II by oxidative stress in cyanobacteria. Photosyn. Res. 84 (1–3), 1–7.
- Paerl, H.W., Huisman, J., 2008. Blooms like it hot. Science 320, 57-58.
- Peng, G., Martin, R.M., Dearth, S.P., Sun, X., Boyer, G.L., Campagna, S.R., Lin, S., Wilhelm, S.W., 2018. Seasonally relevant cool temperatures interact with N chemistry to increase microcystins produced in lab cultures of *Microcystis aeruginosa* NIES-843. Environ. Sci. Technol. 52 (7), 4127–4136.
- Phelan, R.R., Downing, T.G., 2011. A growth advantage for microcystin production by Microcystis PCC7806 under high light. J. Phycol. 47 (6), 1241–1246.
- Rinta-Kanto, J.M., Konopko, E.A., DeBruyn, J.M., Bourbonniere, R.A., Boyer, G.L., Wilhelm, S.W., 2009. Lake Erie *Microcystis*: relationship between microcystin production, dynamics of genotypes and environmental parameters in a large lake. Harmful Algae 8 (5), 665–673.
- Ritter, S.P.A., Lewis, A.C., Vincent, S.L., Lo, L.L., Cunha, A.P.A., Chamot, D., Ensminger, I., Espie, G.S., Owttrim, G.W., 2020. Evidence for convergent sensing of multiple abiotic stresses in cyanobacteria. Biochim. Biophys. Gen. Sub. 1864 (1), 129462
- Schuurmans, J.M., Brinkmann, B.W., Makower, A.K., Dittmann, E., Huisman, J., Matthijs, H.C.P., 2018. Microcystin interferes with defense against high oxidative stress in harmful cyanobacteria. Harmful Algae 78, 47–55.
- Sevilla, E., Bes, M.T., González, A., Peleato, M.L., Fillat, M.F., 2019. Redox-Based Transcriptional regulation in prokaryotes: revisiting model mechanisms. Antioxid. Redox Signal. 30 (13), 1651–1696.
- Stark, G.F., Truchon, A.R., Dittmann, E., Wilhelm, S.W., 2023. Closed circular genome sequence of a Microcystis aeruginosa PCC7806 -mcyB (UTK) nontoxic mutant. Microbiol. Resour. Announc. https://doi.org/10.1128/MRA.00700-23.
- Steffen, M.M., Dearth, S.P., Dill, B.D., Li, Z., Larsen, K.M., Campagna, S.R., Wilhelm, S. W., 2014. Nutrients drive transcriptional changes that maintain metabolic homeostasis but alter genome architecture in *Microcystis*. ISME J. 8 (10), 2080–2092.
- Suzuki, I., Kanesaki, Y., Mikami, K., Kanehisa, M., Murata, N., 2001. Cold-regulated genes under control of the cold sensor Hik33 in *Synechocystis*. Mol. Microbiol. 40 (1), 235–244.
- Van de Waal, D.B., Verspagen, J.M.H., Finke, J.F., Vournazou, V., Immers, A.K., Kardinaal, W.E.A., Tonk, L., Becker, S., Van Donk, E., Visser, P.M., Huisman, J., 2011. Reversal in competitive dominance of a toxic versus non-toxic cyanobacterium in response to rising CO<sub>2</sub>. ISME J. 5 (9), 1438–1450.
- Watanabe, M.M., Ichimura, T., 1977. Fresh-and salt-water forms of *Spirulina platensis* in axenic cultures. Bull. Jpn. Soc. Phycol. 371–377.
- Wetzel, R.G., 2001. Limnology: Lake and River Ecosystems, 3rd edition. Elsevier Science. https://doi.org/10.1016/C2009-0-2112-6.
- Wilhelm, S.W., Boyer, G.L., 2011. Healthy competition. Nat. Clim. Change 1 (6), 300–301.
- Wilhelm, S.W., Bullerjahn, G.S., McKay, R.M.L., 2020. The complicated and confusing ecology of *Microcystis* blooms. mBio 11 (3), e00529, 20.
- Williams, P.W., Peter, D.J., 1989. Control of excitation energy distribution in cyanobacteria: sensitivity to uncouplers and ATP synthase inhibitors. Biochimica et Biophysica Acta (BBA) 1015, 121–130.

- Zhang, Z., Pendse, N.D., Phillips, K.N., Cotner, J.B., Khodursky, A., 2008. Gene expression patterns of sulfur starvation in *Synechocystis* sp. PCC 6803. Bmc Genomics [Electronic Resource] 9, 344.
- Zhao, L., Song, Y.G., Li, L., Gan, N.Q., Brand, J.J., Song, L., 2018. The highly heterogeneous methylated genomes and diverse restriction-modification systems of bloom-forming *Microcystis*. Harmful Algae 75, 87–93.
- Zilliges, Y., Kehr, J.-C., Meissner, S., Ishida, K., Mikkat, S., Hagemann, M., Kaplan, A., Börner, T., Dittmann, E., 2011. The cyanobacterial hepatotoxin microcystin binds to proteins and increases the fFitness of *Microcystis* under oxidative stress conditions. PLoS One 6 (3), e17615.